

# Preparation of high fidelity entangled cat states with composite pulses

Ge-Ge Gu,<sup>1,2</sup> Dong-Sheng Li,<sup>1,2</sup> Ye-Hong Chen,<sup>1,2,3,\*</sup> Bi-Hua Huang,<sup>1,2,†</sup> and Yan Xia<sup>1,2,‡</sup>

<sup>1</sup>*Fujian Key Laboratory of Quantum Information and Quantum Optics, Fuzhou University, Fuzhou 350108, China*

<sup>2</sup>*Department of Physics, Fuzhou University, Fuzhou 350108, China*

<sup>3</sup>*Theoretical Quantum Physics Laboratory, Cluster for Pioneering Research, RIKEN, Wako-shi, Saitama 351-0198, Japan*

We propose a protocol for the preparation of high-fidelity entangled cat states with composite pulses. The physical model contains two Kerr-nonlinear resonators and a cavity. By properly designing the parameters, each Kerr-nonlinear resonator is confined in the cat-state subspace and the entangled cat states can be generated efficiently. We introduce composite two-photon drives with multiple amplitudes and frequencies to improve the fidelity of the entangled cat states in the presence of parameter errors. The performance of the protocol is estimated by taking into account the parametric errors and decoherence. Numerical simulation results show that, the protocol is insensitive to timing error and detuning error, and has strong robustness to decoherence. We hope the protocol may provide a method for preparing stable entangled cat states.

## INTRODUCTION

Quantum computers, which utilize entanglement superposition properties for information processing, possess the potential to outperform classical computers on some certain problems [1–5], such as searching unsorted databases [5]. However, quantum computers also face many challenges. For example, the experimental operating and environment noise may cause errors, especially on large-scale quantum computing [6, 7]. Thus, quantum computing and its scaling will be limited. To reduce error rate, protocols for quantum error correction have been developed in the past decades [3, 8–13]. Encoding quantum information onto bosonic systems is beneficial to quantum error correction in some aspects [14–20]. For example, bosonic systems can provide infinitely large Hilbert space, which could be used to effectively protect and process quantum information [14, 15].

Cat-state qubits are one of the promising bosonic quantum qubits in quantum information processing [17, 21–25], whose two logical qubits are usually represented by two orthogonal cat states (i.e., superposition of coherent states) [26–29]. Cat-state qubits have many unique advantages. For instance, they are noise biased [14, 16]. The phase-flip error can be effectively suppressed, only the bit-flip error needs to be concerned in error correction. Thus, the number of building blocks for error correction can be significantly reduced [13, 15, 18, 30]. In addition, cat qubits have an enhanced lifetime with error corrections [31, 32]. Therefore, cat-state qubits have received much attention and many protocols in view of cat-state qubits have been proposed, such as nonadiabatic geometric quantum computation with cat-state qubits [28] and one-step parity measurement of  $N$  cat-state qubits [32]. Entangled cat states are also important for the demonstration of the fundamentals of quantum physics, and have wide applications in modern quantum technologies [18, 27]. Protocols have been presented for producing entangled cat states, such as

the generation of giant entangled cat states [27] and the preparation of multidimensional entangled cat states in cavity quantum electrodynamics (QED) [19, 33].

In this paper, we consider to use the Mølmer-Sørensen (MS) entangling gate for the preparation of entangled cat states [34, 35]. The MS entangling gate has some specific characteristics. Firstly, it makes qubits independent of the decoherence of the motion mode [34–36]. Secondly, it possesses a built-in noise-resilience feature against certain types of local noise [18]. Therefore, the MS entangling gate has become an important resource and inspired a wide range of research interests [5, 36–42]. For example, in 2021, Chen *et al.* proposed that entangled cat states can be prepared by using cat-code MS gate [18]. However, the protocol [18] could be sensitive to timing error. We note that some kind of composite pulses can play a role in robust control of quantum system and reduce errors [42–48]. For example, Haddadfarshi *et al.* pointed out that properly designed polychromatic control pulses can greatly reduce errors [43] and then Webb *et al.* demonstrated the protocol experimentally [44]. Shapira *et al.* generalized the MS entangling gate by using additional frequency components in the laser drive [45]. Wang *et al.* used suitably designed laser pulse with modulated amplitude and phase to improve the fidelity of the MS entangling gate [46].

Inspired by the literatures above in this paper, we propose to use cat-code MS gate to prepare high-fidelity entangled cat states. We introduce a time-independent drive which is constructed by composite two-photon drives with different amplitudes and frequencies. Under such a drive, we can obtain more stable entangled cat states with appropriate parameters. Meanwhile, the sensitivities of the entangled cat states against errors are significantly reduced, and the robustness to decoherence are obviously improved.

The article is organized as follows. In Sec. , we describe the physical model, and give the concrete form of the Hamiltonian. The effective Hamiltonian is obtained by setting appropriate parameters, and the maximum

entangled cat states are prepared with the MS entangling gate. In Sec. , we introduce the composite drives. Then we prepare the entangled cat states under the effective Hamiltonian, and numerically simulate the feasibility of the protocol. In Sec. , we evaluate the performance of the protocol against errors, and discuss the fidelity of the entangled cat states in the presence of the dephasing and single-photon loss. Finally, conclusions are given in Sec. .

### CAT-CODE MS ENTANGLING GATE

The physical model consists of two Kerr-nonlinear cavities ( $\mathcal{A}_1, \mathcal{A}_2$ ) with the same frequency  $\omega$ , and another cavity ( $\mathcal{A}_0$ ) with frequency  $\omega_0$ . The Hamiltonian of this system in the interaction picture is given by (assume  $\hbar = 1$ )

$$H = \sum_{k=1,2} H_k^{\text{Kerr}} + H_I. \quad (1)$$

The interaction Hamiltonian  $H_I$  is [18]

$$H_I = \sum_{k=1,2} J a_k a_0^\dagger e^{i\Delta t} + \text{H.c.}, \quad (2)$$

where  $J$  is the coupling strength,  $a_k (k = 1, 2)$  is the annihilation operator of the Kerr-nonlinear resonator,  $a_0$  is the annihilation operator of the cavity, and  $\Delta = \omega_0 - \omega$  is the detuning. Each Kerr-nonlinear resonator is resonantly driven by a single-mode two-photon squeezing drive with frequency  $\omega_p = 2\omega$  and amplitude  $\Omega_p$ . The Hamiltonian of the Kerr parametric oscillators (KPOs)  $H_k^{\text{Kerr}}$  in Eq. (1) is [13, 49]

$$H_k^{\text{Kerr}} = -K a_k^{\dagger 2} a_k^2 + (\Omega_p a_k^2 + \Omega_p^* a_k^{\dagger 2}), \quad (3)$$

where  $K$  is Kerr nonlinearity coefficient [50, 51]. To construct cat-state qubits, the Hamiltonian  $H_k^{\text{Kerr}}$  in Eq. (3) can be rewritten as:

$$H_k^{\text{Kerr}} = -K(a_k^{\dagger 2} - \frac{\Omega_p^*}{K})(a_k^2 - \frac{\Omega_p}{K}) + \frac{|\Omega_p|^2}{K}. \quad (4)$$

Equation (4) clearly shows that when  $\alpha = \sqrt{\frac{\Omega_p}{K}}$ , the two coherent states  $|\pm\alpha\rangle$  are degenerate eigenstates of the annihilation operator  $a_k$ . Therefore, the superpositions of the coherent states [13, 14, 49, 52]

$$|C_{\pm}\rangle_k = N_{\pm}(|\alpha\rangle_k \pm |-\alpha\rangle_k), \quad (5)$$

are also the degenerate eigenstates of  $H_k^{\text{Kerr}}$ . Here  $N_{\pm}$  are normalization coefficients. For simplicity, we set the parameters  $\{K, \Omega_p, J, \Delta\} > 0$  and  $\alpha = \alpha^* > 0$ .

The subspace composed by  $|C_{\pm}\rangle_k$  is called the cat-state subspace, which is separated from the other subspaces

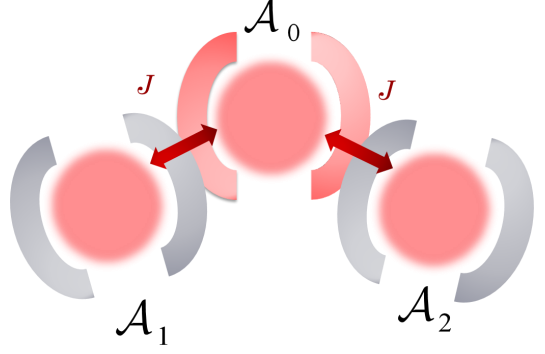


FIG. 1. Two Kerr-nonlinear resonators ( $\mathcal{A}_1, \mathcal{A}_2$ ) are coupled to a cavity ( $\mathcal{A}_0$ ) with a coupling strength of  $J$ , and each Kerr nonlinear resonator is driven by a two-photon drive with a frequency  $\Omega_p$ .

with an energy gap  $E_{\text{gap}} \simeq 4K\alpha^2$  [18]. For large  $\alpha$ , the annihilation operator  $a_k$  only causes the flip between the two cat states, i.e.,

$$a_k |C_{\pm}\rangle_k \simeq \alpha |C_{\mp}\rangle_k. \quad (6)$$

When the condition  $E_{\text{gap}} \gg J$  is satisfied, the transition probability from the ground states  $|C_{\pm}\rangle_k$  to the excited states is extremely small [18]. Therefore, the dynamics of the system can be restricted in the cat-state subspace with the effective Hamiltonian

$$H_{\text{eff}} \approx \sum_{k=1,2} \frac{\Omega_p^2}{K} (|C_-\rangle_k \langle C_-| + |C_+\rangle_k \langle C_+|) + J\alpha [ |C_+\rangle_k \langle C_-| (a_0 e^{-i\Delta t} + a_0^\dagger e^{i\Delta t}) + \text{H.c.}] \quad (7)$$

The first term in the right-hand side of Eq. (7) can be dropped because it is the identity matrix ( $|C_-\rangle_k \langle C_-| + |C_+\rangle_k \langle C_+|$ ) of the subspace. We define Pauli matrices  $\sigma_k^+ = |C_-\rangle_k \langle C_+|$  and  $\sigma_k^- = |C_+\rangle_k \langle C_-|$ . Then the Hamiltonian  $H_{\text{eff}}$  in Eq. (7) reduces to

$$H_{\text{eff}} = 2J\alpha S_x (a_0 e^{-i\Delta t} + a_0^\dagger e^{i\Delta t}), \quad (8)$$

where  $S_x = \frac{1}{2} \sum_{k=1,2} (\sigma_k^+ + \sigma_k^-)$ .

To well understand the evolution of the system, the exact solution of the evolution operator based on the effective Hamiltonian  $H_{\text{eff}}$  can be calculated with the Magnus expansion [53, 54]:

$$U(t) = \exp\{-i[(\chi(t)a_0^\dagger + \text{H.c.})S_x + \beta(t)S_x^2]\}, \quad (9)$$

$$\begin{aligned} \chi(t) &= \frac{2iJ\alpha}{\Delta} [1 - \exp(i\Delta t)], \\ \beta(t) &= \left(\frac{2J\alpha}{\Delta}\right)^2 (\sin \Delta t - \Delta t). \end{aligned} \quad (10)$$

Note that a large detuning  $\Delta$  is necessary for the Magnus expansion to proceed. Setting  $t = T = 2\pi/\Delta$ , there has

$\chi(T) = 0$  and  $\beta(T) = (\frac{2J\alpha}{\Delta})^2 \cdot (-2\pi)$ . When choosing the parameter  $\Delta = 4J\alpha$ , then  $\beta(T) = -\frac{\pi}{2}$ . Thus the evolution operator at time  $T$  reads

$$U(T) = \exp(i\frac{\pi}{2}S_x^2). \quad (11)$$

The  $U(T)$  in Eq. (11) is the well-known MS entangling gate [35]. The MS entangling gate is an important physical resource in quantum computing, for example, it can be applied to the steps of marking and state amplification in Grover's quantum search algorithm [5, 55–59]. Under the action of  $U(T)$ , we can realize the preparation of the entangled cat states. As shown in Eq. (12), the left side of Eq. (12) are the four different initial states (the input states), the right side are the corresponding maximum entangled cat states (the output state) obtained via  $U(T)$  [18, 34].

$$\begin{aligned} |C_+\rangle|C_+\rangle|0\rangle &\rightarrow \frac{1}{\sqrt{2}}(|C_+\rangle|C_+\rangle|0\rangle + i|C_-\rangle|C_-\rangle|0\rangle), \\ |C_-\rangle|C_-\rangle|0\rangle &\rightarrow \frac{1}{\sqrt{2}}(|C_-\rangle|C_-\rangle|0\rangle + i|C_+\rangle|C_+\rangle|0\rangle), \\ |C_+\rangle|C_-\rangle|0\rangle &\rightarrow \frac{1}{\sqrt{2}}(|C_+\rangle|C_-\rangle|0\rangle - i|C_-\rangle|C_+\rangle|0\rangle), \\ |C_-\rangle|C_+\rangle|0\rangle &\rightarrow \frac{1}{\sqrt{2}}(|C_-\rangle|C_+\rangle|0\rangle - i|C_+\rangle|C_-\rangle|0\rangle) \end{aligned} \quad (12)$$

For convenience, the initial state of the system is set as  $|\Psi_{in}\rangle = |C_+\rangle|C_+\rangle|0\rangle$ , and the corresponding entangled cat state is  $|\Psi_{out}\rangle = \frac{1}{\sqrt{2}}(|C_+\rangle|C_+\rangle|0\rangle + i|C_-\rangle|C_-\rangle|0\rangle)$  in this manuscript. All numerical simulation results in this section are obtained by using the full Hamiltonian given by Eq. (1). Here, the fidelity of entangled state is given by  $F = \langle \Psi | \rho | \Psi \rangle$ , where  $|\Psi\rangle$  is the target entangled cat state i.e.,  $|\Psi_{out}\rangle$ , and  $\rho$  is the density operator. The experimental parameters are chosen as  $\alpha = 2$ , the Kerr nonlinearity  $K/2\pi = 20\text{MHz}$  [60],  $\Omega_p = K\alpha^2$ ,  $J = 2\pi\text{MHz}$ , and  $\Delta = 4J\alpha$ .

In Fig. 2(a), we plot the time evolutions of the states  $|C_+\rangle|C_+\rangle|0\rangle$  and  $|C_-\rangle|C_-\rangle|0\rangle$ . As is shown, the populations of both states are close to 50% around the gate time  $T$ . This means that the protocol is feasible, and the maximum entangled cat state can be successfully prepared when  $t = T$ . However, the high-fidelity entangled cat state can only exist when the time is extremely close to  $T$ . When the timing error  $\delta_t$  deviates from 0, the fidelity of the entangled cat state  $|\Psi_{out}\rangle$  drops significantly, which can be seen in Fig. 2(b). Here, the relative error of the parameter  $x$  is defined via  $\delta_x = (x' - x)/x$ , in which  $x'$  denotes the actual value and  $x$  is the ideal value.

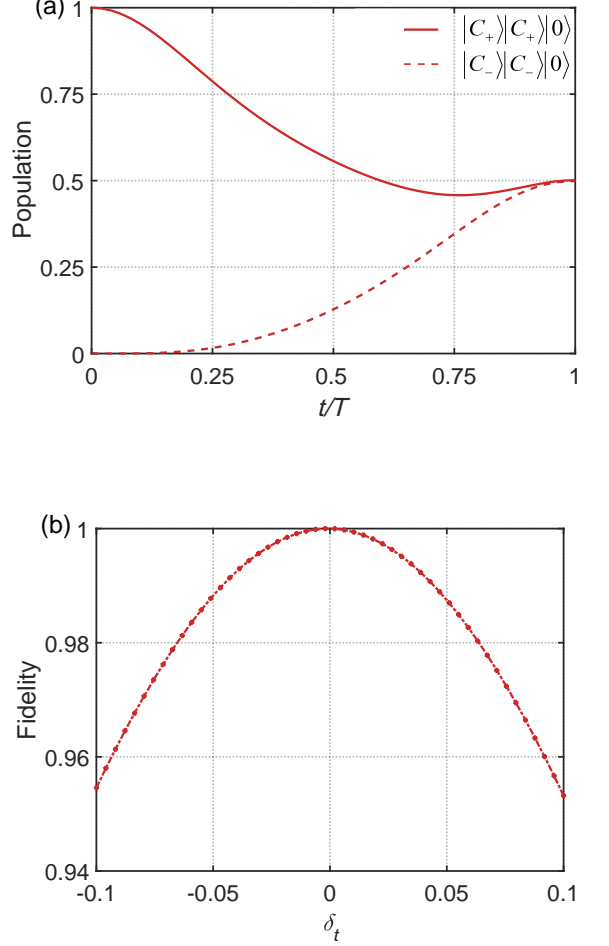


FIG. 2. (a) Population evolution of the cat states. The solid line represents the state  $|C_+\rangle|C_+\rangle|0\rangle$ , and the dotted line represents the state  $|C_-\rangle|C_-\rangle|0\rangle$ . (b) The fidelity against timing error  $\delta_t$ , error range is selected for  $[-0.1, 0.1]$ . The experimental parameters are set as  $\alpha = 2$ ,  $T = 2\pi/\Delta$ , the Kerr nonlinearity  $K/2\pi = 20\text{MHz}$ , the driving amplitude  $\Omega_p = K\alpha^2$ ,  $J = 2\pi\text{MHz}$ , and  $\Delta = 4J\alpha$ .

## PREPARATION OF HIGH-FIDELITY ENTANGLED CAT STATE

As shown in the second section, the fidelity of the entangled cat state is relatively sensitive to time error. In order to obtain stable and high-fidelity entangled cat state, we introduce composite two-photon squeezing drives with frequency  $\omega_n$  and amplitude  $\Omega_n$ . Then the total Hamiltonian  $H$  in Eq. (1) changes to

$$H' = \sum_{k=1,2} H_k^{\text{Kerr}'} + H_I, \quad (13)$$

$$H_k^{\text{Kerr}'} = -K a_k^{\dagger 2} a_k^2 + (\Omega_p a_k^2 + \Omega_p^* a_k^{\dagger 2})$$

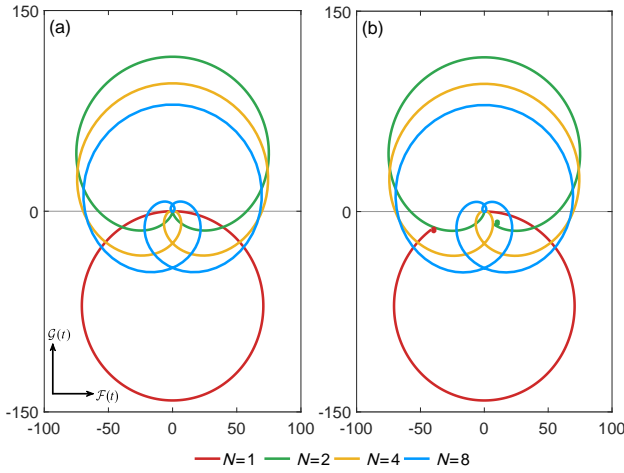


FIG. 3. Phase-space trajectories of  $\mathcal{F}(t)$  and  $\mathcal{G}(t)$  for  $N \in [1, 2, 4, 8]$ . (a) without errors, (b) with 10% timing error.

$$+ \sum_{n=1}^N (\Omega_n a_k^{\dagger 2} e^{i\delta_n t} + \Omega_n^* a_k^2 e^{-i\delta_n t}). \quad (14)$$

The last term in Eq. (14) is the additional composite drives, and  $\delta_n = \omega_n - \omega$  is the detuning of the  $n$ th two-photon drive. According to effective Hamiltonian theory [61], the effective Hamiltonian in the limit of large detunings can be written as

$$H_{\text{eff},N}(t) = \sum_{n=1}^N \frac{4J\Omega_n}{\varepsilon_n} [a_k^\dagger a_0^\dagger e^{i(\Delta-\delta_n)t} + \text{H.c.}], \quad (15)$$

where  $\frac{1}{\varepsilon_n} = (\frac{1}{\Delta} + \frac{1}{\delta_n})$ . Similar to the derivation from Eq. (1) to Eq. (8), we can get a new effective Hamiltonian by restricting the Hamiltonian  $H_{\text{eff},N}(t)$  to the cat-state subspace

$$H'_{\text{eff},N}(t) = 2J\alpha S_x \sum_{n=1}^N \frac{4\Omega_n}{\varepsilon_n} [a_0^\dagger e^{i(\Delta-\delta_n)t} + \text{H.c.}]. \quad (16)$$

For simplicity, we define  $\frac{4\Omega_n}{\varepsilon_n} = r_n$  and  $\zeta = (\Delta - \delta_n)/n$  with  $n = 1, 2, 3, \dots, N$ . Then the effective Hamiltonian  $H'_{\text{eff},N}(t)$  can be expressed as

$$H_{\text{MS},N}(t) = 2J\alpha S_x \sum_{n=1}^N r_n (a_0 e^{in\zeta t} + a_0^\dagger e^{-in\zeta t}). \quad (17)$$

To understand the construction of composite pulses, we introduce the dimensionless position operator  $x = \frac{1}{\sqrt{2}}(a_0 + a_0^\dagger)$  and the momentum operator  $p = \frac{i}{\sqrt{2}}(a_0^\dagger - a_0)$ . The effective Hamiltonian in Eq. (17) can be reformulated as

$$\mathcal{H}_{\text{MS},N}(t) = f(t)S_x x + g(t)S_x p. \quad (18)$$

where  $f(t) = 2\sqrt{2}J\alpha \sum_{n=1}^N \cos(n\zeta t)$  and  $g(t) = -2\sqrt{2}J\alpha \sum_{n=1}^N \sin(n\zeta t)$ . The propagator for the Hamiltonian in Eq. (18) can be expressed as [35, 45]

$$\mathcal{U}(t) = e^{-i\mathcal{F}(t)S_x x} e^{-i\mathcal{G}(t)S_x p} e^{-i\mathcal{A}(t)S_x^2}, \quad (19)$$

where

$$\begin{aligned} \mathcal{F}(t) &= \int_0^t f(t') dt' = \frac{2\sqrt{2}J\alpha}{\zeta} \sum_{n=1}^N \frac{r_n}{n} \sin(n\zeta t), \\ \mathcal{G}(t) &= \int_0^t g(t') dt' = \frac{2\sqrt{2}J\alpha}{\zeta} \sum_{n=1}^N \frac{r_n}{n} [\cos(n\zeta t) - 1], \\ \mathcal{A}(t) &= - \int_0^t \mathcal{F}(t') \mathcal{G}(t') dt', \end{aligned} \quad (20)$$

and  $\{r_n\}_{n=1}^N$  is a numerical set of  $r_n$  when  $N$  takes different values [45]

$$r_n = (-1)^{N-n} \frac{N!}{2^N} \sqrt{\frac{2\sqrt{\pi}}{(N-1)\Gamma(N+\frac{1}{2})}} \frac{(N-1)!}{(N-n)!(n-1)!}. \quad (21)$$

Here  $\Gamma(a) = \int_0^\infty e^{-x} x^{a-1} dx$ .

As seen in Eq. (19), the evolution of the operator  $\mathcal{U}(t)$  follows the trajectory with dimensionless coordinates  $\mathcal{F}(t)$  and  $\mathcal{G}(t)$  in the  $x - p$  phase-space. Equation (20) shows that  $\mathcal{F}(t)$  and  $\mathcal{G}(t)$  are respectively the integrations of  $f(t)$  and  $g(t)$  [35, 43]. Ideally, when the time  $t = \tau = \frac{2\pi}{\zeta}$ ,  $\mathcal{F}(\tau) = 0$ ,  $\mathcal{G}(\tau) = 0$ , and the phase-space trajectory of  $(\mathcal{F}(t), \mathcal{G}(t))$  is closed as seen in Fig. 3(a). Meanwhile, the operator  $\mathcal{U}(\tau) = e^{-i\mathcal{A}(\tau)S_x^2}$ , that is, only the internal spin evolution is retained. However, errors will lead to the phase-space trajectory not closed completely, which in turn can cause infidelity of entangled cat states [44, 46, 62]. We can see from Fig. 3(b), the circular trajectory becomes more complete with the increase of  $N$ . In other words, we can reduce errors of the entangled cat states by increasing  $N$ .

The full Hamiltonian of the optimized protocol is written as

$$\begin{aligned} H_N(t) &= \sum_{k=1,2} [-K a_k^{\dagger 2} a_k^2 + (\Omega_p a_k^2 + \Omega_p^* a_k^{\dagger 2})] \\ &+ \sum_{k=1,2} [J_N(t) a_k a_0^\dagger \exp(i\Delta t) + \text{H.c.}], \end{aligned} \quad (22)$$

where  $J_N(t) = J e^{-i\Delta t \sum_{n=1}^N r_n e^{in\zeta t}}$  is the composite drive. If the condition  $\Delta = \zeta$  is satisfied,  $J_1(t) = J$ , the case  $N = 1$  corresponds to the unoptimized protocol, which is discussed in the second section.

In Fig. 4, we plot the population evolutions of the cat states with different  $N$  ( $N = 1, 2, 4, 8$ ). We can see from Fig. 4 that the curves become more flat near time  $T$  with the increase of  $N$ . This means that more stable entangled cat state can be obtained by simply increasing  $N$ . Here, the parameters  $\{\alpha, K, \Omega_p, \Delta\}$  are same as Fig. 2, and  $\zeta = \Delta$ .

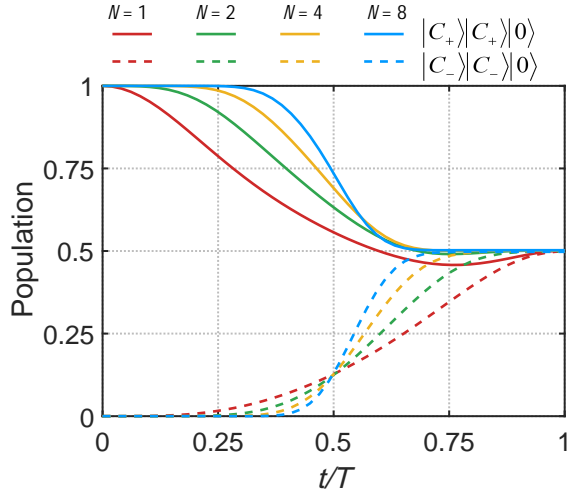


FIG. 4. The population evolution of cat states, the values of  $N \in 1, 2, 4, 8$ . The solid line represents the state  $|C_+\rangle|C_+\rangle|0\rangle$ , and the dotted line represents the state  $|C_-\rangle|C_-\rangle|0\rangle$ .

### ERROR AND DECOHERENCE ANALYSIS

In this section, we will investigate the performance of the optimized protocol. Specifically, we discuss the effects of parameters errors on the fidelity of entangled cat state in the Sec. . Then we analyze the robustness of the entangled cat state to dephasing and single-photon losses in Sec. . Here, we choose the values  $N \in [1, 4, 8]$ .

#### Robustness against parametric errors

It is inevitable that some parametric errors will cause infidelity in the entangled cat states because of the imperfect experimental operations. In this part, with the help of the numerical simulation, we will show the sensitivity of the protocol against parameter errors i.e., timing error  $\delta_t$ , detuning error  $\delta_\Delta$ , and coupling error  $\delta_J$ .

In Fig. 5(a), we numerically study the robustness of the protocol for timing error  $\delta_t$ . The error range is  $\delta_t \in [-0.1, 0.1]$  and the curve for  $N = 1$  corresponds to the unoptimized one. As expected, when  $N$  takes different value, the fidelity of the entangled cat state changes. Comparing the curves with  $N = 1$  and  $N = 4$ , we can see the fidelity has been greatly improved. When  $N$  is set to a larger value i.e.,  $N = 8$ , the fidelity of entangled cat state is almost unaffected by timing error. That is, the protocol can enhance the robustness against timing error.

In actual experiments, imperfect experimental operations may cause inevitable detuning errors. We consider the range of detuning error  $\delta_\Delta$  as  $[-0.1, 0.1]$ , and plot the fidelity versus detuning error  $\delta_\Delta$  in the Fig. 5(b). It can

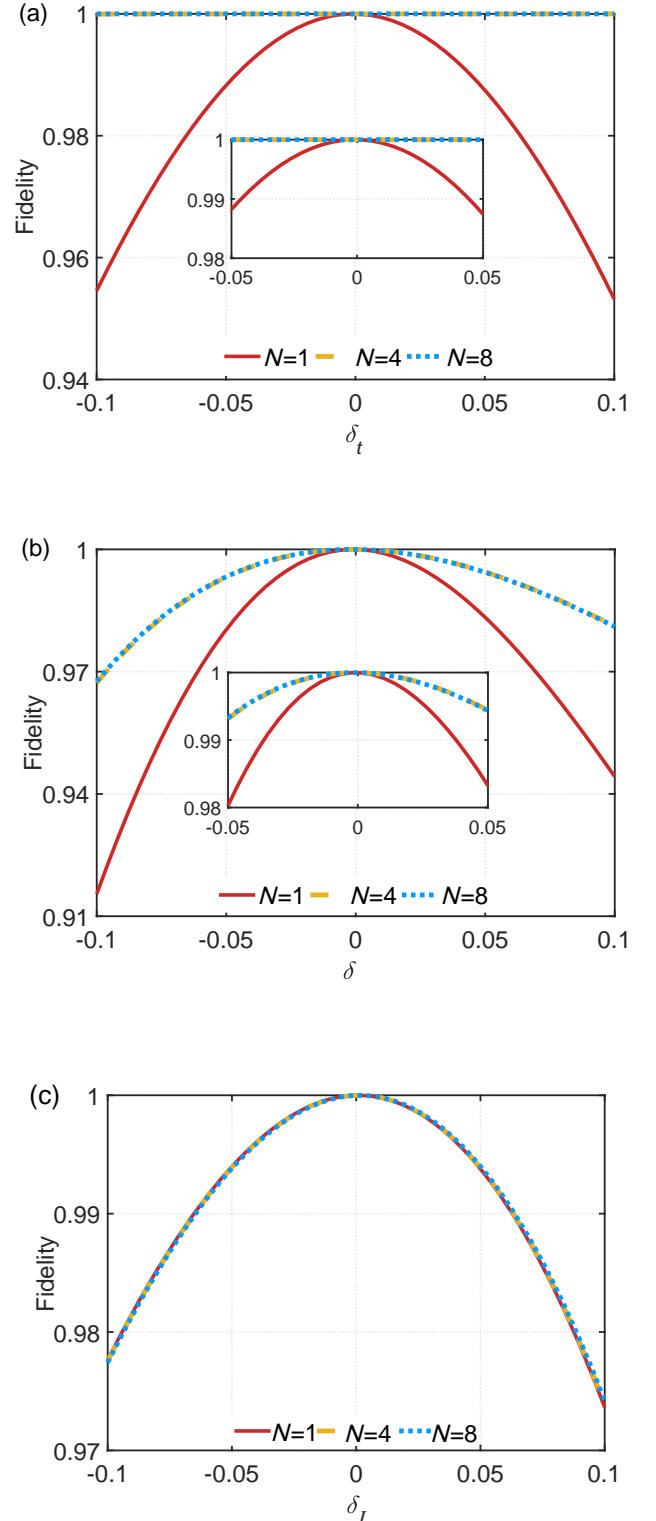


FIG. 5. Fidelity versus parameter errors. (a) timing error, (b) detuning error, (c) coupling error. In figures (a) and (b), increasing  $N$  leads to a flatter response to control errors, the robustnesses against parameters errors are enhanced. The other parameters are the same as in Fig. 4

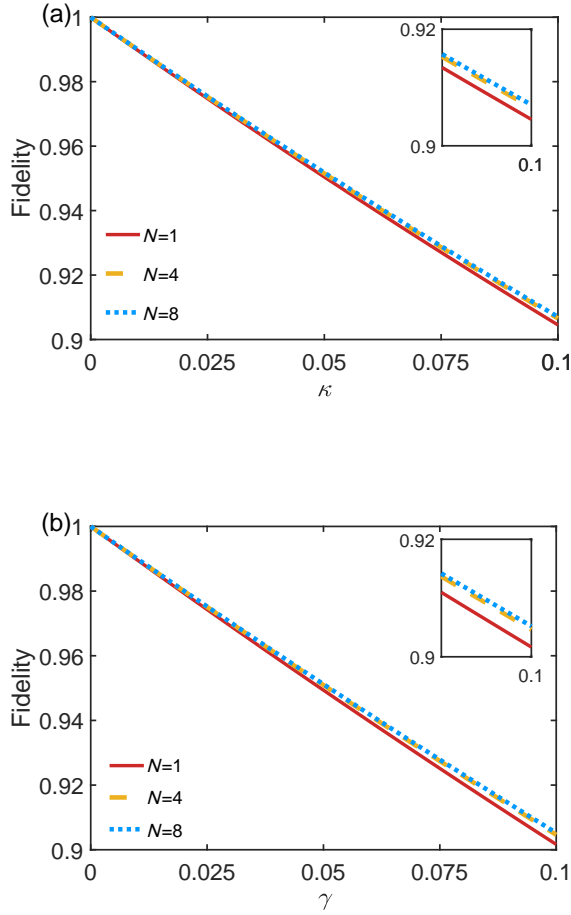


FIG. 6. (a) Fidelity versus the single-photon losses rate  $\kappa \in [0, 0.1]$  MHz and the dephasing rate  $\gamma = 0$ . (b) Fidelity versus dephasing  $\gamma \in [0, 0.1]$  MHz with single-photon losses rate  $\kappa = 0$ .

be seen from the figure that the fidelity of the entangled cat state for  $N > 1$  is much higher than that with  $N = 1$ . The inset in Fig. 5(b) shows that when the error range is  $[-0.05, 0.05]$ , the fidelities are large than 0.99 when  $N > 1$ . This indicates that the increase of  $N$  can reduce the sensitivity to detuning errors.

Figure 5(c) shows the fidelity against coupling error  $\delta_J$ . As shown in Fig. 5(c), the fidelity is unaffected by the values of  $N$ , and the value of fidelity always greater than 0.97. That shows that the protocol cannot improve the robustness against errors in the coupling.

### Robustness against decoherence

In the process of gate operation, decoherence can cause infidelity. For the system discussed, we consider two types of noise: single-photon losses and pure dephasing.

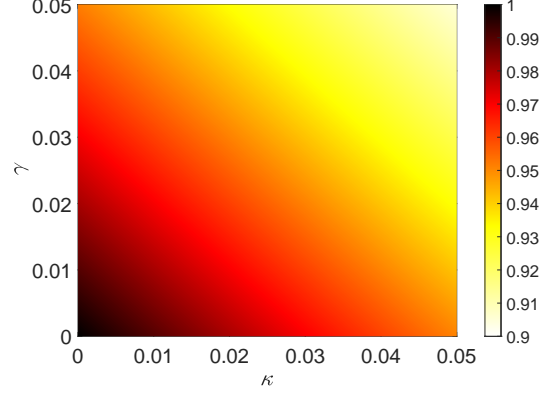


FIG. 7. Fidelity of the optimized protocol with  $N = 8$  versus  $\kappa = \gamma \in [0, 0.05]$  MHz. Other parameters remain unchanged.

The master equation of the system can be written as:

$$\begin{aligned} \dot{\rho} = & -i[H, \rho] + \kappa_0 D[a_0] \rho + \gamma_0 D[a_0^\dagger a_0] \rho \\ & + \sum_{k=1,2} \kappa_k D[a_k] \rho + \gamma_k D[a_k^\dagger a_k] \rho, \end{aligned} \quad (23)$$

where  $\rho$  is the density operator of the system,  $D[o]\rho = o\rho o^\dagger - \frac{1}{2}(o^\dagger o\rho + \rho o^\dagger o)$ . For simplicity, we assume that  $\kappa_k = \kappa$  ( $k = 1, 2$ ) is the single-photon losses rate, and  $\gamma_k = \gamma$  is the pure dephasing rate. Note that the influence of decoherence in the cavity mode  $\mathcal{A}_0$  is different from those in the KPOs. The decoherence of the cavity mode  $\mathcal{A}_0$  can be adiabatically eliminated for large  $\Delta$  [18], so the system is insensitive to the decoherence of  $\mathcal{A}_0$ . In the numerical simulation, we set  $\kappa_0 = \kappa$  and  $\gamma_0 = \gamma$  for convenience. To well understand the effect of decoherence, we project the system onto the eigenstates of  $H_k^{\text{Kerr}}$ . Here, the projection operator of the KPOs is

$$P = \sum_{k=1,2} [|C_\pm\rangle_k \langle C_\pm| + \sum_{v=1}^{\infty} |\psi_\pm^{e,v}\rangle_k \langle \psi_\pm^{e,v}|], \quad (24)$$

where  $|\psi_\pm^{e,v}\rangle_k = N_\pm^e [D_k(\alpha) \mp |D_k(-\alpha)|] |v\rangle_k$ ,  $v$  represents the level of the excited states. Then the master equation becomes

$$\begin{aligned} \dot{\rho} \simeq & -i[PHP, \rho] + \kappa_0 D[a_0] \rho + \gamma_0 D[a_0^\dagger a_0] \rho \\ & + \sum_{k=1,2} \kappa_k D[P a_k P] \rho + \sum_{k=1,2} \gamma_k D[P a_k^\dagger a_k P] \rho \end{aligned} \quad (25)$$

When  $\gamma_k, \kappa_k$  are much smaller than the energy gap  $E_{\text{gap}}$ , the dynamics of the system is still well confined to the cat-subspace [13, 14, 49, 52]. For large  $\alpha$ , the influence of the single-photon losses in the KPOs is described by the penultimate term in Eq. (25)

$$D'[a_k] = D[P a_k P]$$

$$\begin{aligned}
\simeq & \alpha^2 D [\sqrt{\tanh \alpha^2} |C_+\rangle_k \langle C_-| + \sqrt{\coth \alpha^2} |C_-\rangle_k \langle C_+|] \\
& + D [\sqrt{\frac{N_+}{N_+^e}} |C_+\rangle_k \langle \psi_+^{e,1}| + \sqrt{\frac{N_-}{N_-^e}} |C_-\rangle_k \langle \psi_-^{e,1}|] \\
& + \alpha^2 D [\sqrt{\frac{N_-}{N_+^e}} |\psi_-^{e,1}\rangle_k \langle \psi_+^{e,1}| + \sqrt{\frac{N_+^e}{N_-^e}} |\psi_+^{e,1}\rangle_k \langle \psi_-^{e,1}|], \tag{26}
\end{aligned}$$

where  $|\psi_{\pm}^{e,1}\rangle_k$  are the first-excited eigenstates of the Hamiltonian  $H_k^{\text{Kerr}}$ . Note that the highly excited eigenstates of KPOs are not excited in the presence of single-photon losses. Therefore, we only consider the first-excited eigenstates in Eq. (24). The second term in Eq. (26) means that single-photon losses can only cause the transition from the excited eigenstate  $|\psi_{\pm}^{e,1}\rangle_k$  to the ground state  $|C_{\pm}\rangle_k$ . If the KPOs are initially in the cat-state subspace, they always remain in the cat-state subspace. Therefore, we can ignore the last two terms of the Eq. (26) and obtain

$$D'[a_k]\rho \simeq \frac{\alpha^2}{\sqrt{1 - e^{-4\alpha}}} D[\sigma_k^x + ie^{-2\alpha^2} \sigma_k^y] \rho, \tag{27}$$

where  $\sigma_k^x = |C_+\rangle_k \langle C_-| + |C_-\rangle_k \langle C_+|$ ,  $\sigma_k^y = i(|C_-\rangle_k \langle C_+| - |C_+\rangle_k \langle C_-|)$ . Bringing the Eq. (27) into the Eq. (25), we find that in the computational subspace, single-photon losses mainly lead to a bit-flip error  $\sigma_k^x$ , accompanied by an exponentially small phase flip error  $\sigma_k^y$ .

In Fig. 6(a), we plot the fidelity of the single-photon losses for different values of  $N$ . The single-photon losses rate is assumed as  $\kappa \in [0, 0.1]$  MHz, and the dephasing rate is assumed as  $\gamma = 0$ . As can be seen from Fig. 6(a), the increase of  $N$  does not affect the fidelity too much. The fidelities can all reach above 0.9 when  $\kappa = 0.1$  MHz, which means that the optimized protocol still maintains a high fidelity in the presence of the single-photon losses. We also numerically simulate the dependence of the fidelity on the pure dephasing rate in Fig. 6(b) and a similar result can be obtained.

Since single-photon losses and dephasing coexist in the system, so we numerically investigate the effect on the fidelity when single-photon losses and dephasing are present together. In Fig. 7, we plot the fidelity of the optimized protocol with  $N = 8$  versus  $\kappa = \gamma \in [0, 0.05]$  MHz. The result shows that the optimized protocol maintains a high fidelity more than 0.9 even when photon losses and dephasing exist simultaneously.

## CONCLUSION

In conclusion, we have investigated a protocol to use photonic cat-state qubits for preparing high-fidelity entangled cat states. The entangled cat states can

be successfully obtained under the action of the cat-code MS gate. We further adopt composite pulses to improve the fidelity of the entangled cat states. The modulated time-independent composite drives can be realized by introducing composite two-photon squeezing drives. Numerical simulation results show that the protocol can provide strong robustness against timing error. The protocol also exhibits high insensitivity to other parametric errors with proper parameters. Furthermore, under the influence of decoherence, the protocol still maintains a high fidelity. That is, the higher fidelity of the entangled cat states are possible with the larger  $N$  of the parameter. On the other hand, employing composite pulses to prepare entangled states is meaningful to investigate. We hope that the proposal could offer a simple and feasible method for preparing stable and high-fidelity entangled cat states in quantum computation.

Y. Xia was supported by the National Natural Science Foundation of China under Grants Nos. 11575045, 11874114, the Natural Science Funds for Distinguished Young Scholar of Fujian Province under Grant 2020J06011 and Project from Fuzhou University under Grant JG202001-2. Y.-H. Chen was supported by the National Natural Science Foundation of China under Grants No. 12304390.

\* yehong.chen@fzu.edu.cn

† hbh@fzu.edu.cn

‡ xia-208@163.com

- [1] Michael A. Nielsen and Isaac L. Chuang, *Quantum Computation and Quantum Information: 10th Anniversary Edition* (Cambridge University Press, Cambridge, 2012).
- [2] A. Steane, “Quantum computing,” *Rep. Prog. Phys.* **61**, 117–173 (1998).
- [3] M. Kjaergaard, M. E. Schwartz, J. Braumüller, P. Krantz, J. I.-J. Wang, S. Gustavsson, and W. D. Oliver, “Superconducting qubits: Current state of play,” *Ann. Rev. Cond. Matt. Physics* **11**, 369–395 (2020).
- [4] F. Arute, K. Arya, R. Babbush, and et al., “Quantum supremacy using a programmable superconducting processor,” *Nature* **574** (2019).
- [5] K.-A. Brickman, P. C. Haljan, P. J. Lee, M. Acton, L. Deslauriers, and C. Monroe, “Implementation of grover’s quantum search algorithm in a scalable system,” *Phys. Rev. A* **72**, 050306 (2005).
- [6] A. G. Fowler, M. Mariantoni, J. M. Martinis, and A. N. Cleland, “Surface codes: Towards practical large-scale quantum computation,” *Phys. Rev. A* **86**, 032324 (2012).
- [7] D. Litinski, “A game of surface codes: Large-scale quantum computing with lattice surgery,” *Quantum* **3**, 128 (2019).
- [8] P. W. Shor, “Scheme for reducing decoherence in quantum computer memory,” *Phys. Rev. A* **52**, R2493–R2496 (1995).
- [9] A. Y. Kitaev, “Fault-tolerant quantum computation by anyons,” *Ann. Phys.* **303**, 2–30 (2003).

[10] C. Chamberland *et al.*, “Building a fault-tolerant quantum computer using concatenated cat codes,” *PRX Quantum* **3**, 010329 (2022).

[11] S. J. Devitt, W. J. Munro, and K. Nemoto, “Quantum error correction for beginners,” *Rep. Prog. Phys.* **76**, 076001 (2013).

[12] J. Zhang, S. J. Devitt, J. Q. You, and F. Nori, “Holonomic surface codes for fault-tolerant quantum computation,” *Phys. Rev. A* **97**, 022335 (2018).

[13] S. Puri, A. Grimm, P. Campagne-Ibarcq, A. Eickbusch, K. Noh, G. Roberts, L. Jiang, M. Mirrahimi, M. H. Devoret, and S. M. Girvin, “Stabilized cat in a driven nonlinear cavity: A fault-tolerant error syndrome detector,” *Phys. Rev. X* **9**, 041009 (2019).

[14] W. Cai, Y. Ma, W. Wang, C.-L. Zou, and L. Sun, “Bosonic quantum error correction codes in superconducting quantum circuits,” *Fund. Res.* **1**, 50–67 (2021).

[15] J. Guillaud and M. Mirrahimi, “Repetition cat qubits for fault-tolerant quantum computation,” *Phys. Rev. X* **9**, 041053 (2019).

[16] W.-L. Ma, S. Puri, R. J. Schoelkopf, M. H. Devoret, S. M. Girvin, and L. Jiang, “Quantum control of bosonic modes with superconducting circuits,” *Sci. Bull.* **66**, 1789–1805 (2021).

[17] T. C. Ralph, A. Gilchrist, G. J. Milburn, W. J. Munro, and S. Glancy, “Quantum computation with optical coherent states,” *Phys. Rev. A* **68**, 042319 (2003).

[18] Y.-H. Chen, R. Stassi, W. Qin, A. Miranowicz, and F. Nori, “Fault-tolerant multiqubit geometric entangling gates using photonic cat-state qubits,” *Phys. Rev. Appl.* **18**, 024076 (2022).

[19] C.-P. Yang, J.-H. Ni, L. Bin, Y. Zhang, Y. Yu, and Q.-P. Su, “Preparation of maximally-entangled states with multiple cat-state qutrits in circuit qed,” *Fron. Phys.* (2023).

[20] M. H. Michael, M. Silveri, R. T. Brierley, V. V. Albert, J. Salmilehto, L. Jiang, and S. M. Girvin, “New class of quantum error-correcting codes for a bosonic mode,” *Phys. Rev. X* **6**, 031006 (2016).

[21] Z.-Y. Zhou, C. Gneiting, J.-Q. You, and F. Nori, “Generating and detecting entangled cat states in dissipatively coupled degenerate optical parametric oscillators,” *Phys. Rev. A* **104**, 013715 (2021).

[22] Y. Shen, S. M. Assad, N. B. Grosse, X. Y. Li, M. D. Reid, and P. K. Lam, “Nonlinear entanglement and its application to generating cat states,” *Phys. Rev. Lett.* **114**, 100403 (2015).

[23] S.-B. Zheng, “A scheme for the generation of multi-mode schrödinger cat states,” *J. Euro. Opt. Soc. B* **10**, 691 (1998).

[24] L. Li, C.-L. Zou, V. V. Albert, S. Muralidharan, S. M. Girvin, and L. Jiang, “Cat codes with optimal decoherence suppression for a lossy bosonic channel,” *Phys. Rev. Lett.* **119**, 030502 (2017).

[25] Y.-H. Chen, Z.-C. Shi, F. Nori, and Y. Xia, “Error-tolerant amplification and simulation of the ultrastrong-coupling quantum Rabi model,” *Phys. Rev. Lett.* (accepted).

[26] A. Gilchrist, K. Nemoto, W. J. Munro, T. C. Ralph, S. Glancy, S. L. Braunstein, and G. J. Milburn, “Schrödinger cats and their power for quantum information processing,” *J. Opt. B* **6**, S828 (2004).

[27] Y.-H. Chen, W. Qin, X. Wang, A. Miranowicz, and F. Nori, “Shortcuts to adiabaticity for the quantum Rabi model: Efficient generation of giant entangled cat states via parametric amplification,” *Phys. Rev. Lett.* **126**, 023602 (2021).

[28] Y.-H. Kang, Y.-H. Chen, X. Wang, J. Song, Y. Xia, A. Miranowicz, S.-B. Zheng, and F. Nori, “Nonadiabatic geometric quantum computation with cat-state qubits via invariant-based reverse engineering,” *Phys. Rev. Res.* **4**, 013233 (2022).

[29] S. Liu, Y.-H. Chen, Y. Wang, Y.-H. Kang, Z.-C. Shi, J. Song, and Y. Xia, “Generation of cat states by a weak parametric drive and a transitionless tracking algorithm,” *Phys. Rev. A* **106**, 042430 (2022).

[30] M. Mirrahimi, Z. Leghtas, V. V. Albert, S. Touzard, R. J. Schoelkopf, L. Jiang, and M. H. Devoret, “Dynamically protected cat-qubits: a new paradigm for universal quantum computation,” *New J. Phys.* **16**, 045014 (2014).

[31] N. Ofek, R. Petrenko, A. and Heeres, P. Reinhold, Z. Leghtas, B. Vlastakis, Y. Liu, L. Frunzio, S. M. Girvin, L. Jiang, M. Mirrahimi, M. H. Devoret, and R. J. Schoelkopf, “Extending the lifetime of a quantum bit with error correction in superconducting circuits,” *Nature* (2016).

[32] D.-S. Li, Y.-H. Kang, Y.-H. Chen, Y. Liu, C. Zhang, Y. Wang, J. Song, and Y. Xia, “One-step parity measurement of  $n$  cat-state qubits via reverse engineering and optimal control,” *Phys. Rev. A* **109**, 022437 (2024).

[33] Y. Zhang, T. Liu, Y. Yu, and C.-P. Yang, “Preparation of entangled w states with cat-state qubits in circuit qed,” *Quantum Inf. Proc.* (2020).

[34] A. Sørensen and K. Mølmer, “Quantum computation with ions in thermal motion,” *Phys. Rev. Lett.* **82**, 1971–1974 (1999).

[35] A. Sørensen and K. Mølmer, “Entanglement and quantum computation with ions in thermal motion,” *Phys. Rev. A* **62**, 022311 (2000).

[36] A. Mitra, M. J. Martin, G. W. Biedermann, A. M. Marino, P. M. Poggi, and I. H. Deutsch, “Robust mølmer-sørensen gate for neutral atoms using rapid adiabatic rydberg dressing,” *Phys. Rev. A* **101**, 030301 (2020).

[37] S.-L. Zhu, C. Monroe, and L.-M. Duan, “Arbitrary-speed quantum gates within large ion crystals through minimum control of laser beams,” *EPL* **73**, 485 (2006).

[38] T. Choi, S. Debnath, T. A. Manning, C. Figgatt, Z.-X. Gong, L.-M. Duan, and C. Monroe, “Optimal quantum control of multimode couplings between trapped ion qubits for scalable entanglement,” *Phys. Rev. Lett.* **112**, 190502 (2014).

[39] T. J. Green and M. J. Biercuk, “Phase-modulated decoupling and error suppression in qubit-oscillator systems,” *Phys. Rev. Lett.* **114**, 120502 (2015).

[40] C. J. Ballance, T. P. Harty, N. M. Linke, M. A. Sepiol, and D. M. Lucas, “High-fidelity quantum logic gates using trapped-ion hyperfine qubits,” *Phys. Rev. Lett.* **117**, 060504 (2016).

[41] J. P. Gaebler, T. R. Tan, Y. Lin, Y. Wan, R. Bowler, A. C. Keith, S. Glancy, K. Coakley, E. Knill, D. Leibfried, and D. J. Wineland, “High-fidelity universal gate set for  ${}^9\text{Be}^+$  ion qubits,” *Phys. Rev. Lett.* **117**, 060505 (2016).

[42] T. Manovitz, A. Rotem, R. Shani, I. Cohen, Y. Shapira, N. Akerman, A. Retzker, and R. Ozeri, “Fast dynamical

decoupling of the mølmer-sørensen entangling gate,” *Phys. Rev. Lett.* **119**, 220505 (2017).

[43] F. Haddadfarshi and F. Mintert, “High fidelity quantum gates of trapped ions in the presence of motional heating,” *New J. Phys.* **18**, 123007 (2016).

[44] A. E. Webb, S. C. Webster, S. Collingbourne, D. Breaud, A. M. Lawrence, S. Weidt, F. Mintert, and W. K. Hensinger, “Resilient entangling gates for trapped ions,” *Phys. Rev. Lett.* **121**, 180501 (2018).

[45] Y. Shapira, R. Shaniv, T. Manovitz, N. Akerman, and R. Ozeri, “Robust entanglement gates for trapped-ion qubits,” *Phys. Rev. Lett.* **121**, 180502 (2018).

[46] Y. Wang, J.-L. Wu, J.-X. Han, Y.-Y. Jiang, Y. Xia, and J. Song, “Resilient Mølmer-Sørensen gate with cavity qed,” *Phys. Lett. A* **388**, 127033 (2021).

[47] M. Palmero, S. Martínez-Garaot, D. Leibfried, D. J. Wineland, and J. G. Muga, “Fast phase gates with trapped ions,” *Phys. Rev. A* **95**, 022328 (2017).

[48] P. H. Leung, K. A. Landsman, C. Figgatt, N. M. Linke, C. Monroe, and K. R. Brown, “Robust 2-qubit gates in a linear ion crystal using a frequency-modulated driving force,” *Phys. Rev. Lett.* **120**, 020501 (2018).

[49] S. Puri, S. Boutin, and A. Blais, “Engineering the quantum states of light in a Kerr-nonlinear resonator by two-photon driving,” *npj Quantum Inf.* (2017).

[50] A. Miranowicz, J. Bajer, N. Lambert, and F. Liu, Y.-x. and Nori, “Tunable multiphonon blockade in coupled nanomechanical resonators,” *Physical Review A* **93** (2016), 10.1103/physreva.93.013808.

[51] J. Bourassa, F. Beaudoin, Jay M. Gambetta, and A. Blais, “Josephson-junction-embedded transmission-line resonators: From Kerr medium to in-line transmon,” *Phys. Rev. A* **86**, 013814 (2012).

[52] S. Puri, L. St-J., Jonathan A. Gross, A. Grimm, N. E. Frattini, P. S. Iyer, A. Krishna, S. Touzard, L. Jiang, A. Blais, S. T. Flammia, and S. M. Girvin, “Dbias-preserving gates with stabilized cat qubits,” *Sci. Adv.* (2020).

[53] S. Blanes, F. Casas, J. A. Oteo, and J. Ros, “A pedagogical approach to the magnus expansion,” *Euro. J. Phys.* **31**, 907 (2010).

[54] S. Blanes, F. Casas, J. A. Oteo, and J. Ros, “The magnus expansion and some of its applications,” *Phys. Rep.* **470**, 151–238 (2009).

[55] H. Ohno, “Grover’s search with learning oracle for constrained binary optimization problems,” *Quantum Mach. Int.* (2024).

[56] C. Yang, T. Liu, J. Zhu, J. Ren, and H. Chen, “Surface-acoustic-wave computing of the Grover quantum search algorithm with metasurfaces,” *Phys. Rev. Appl.* **15**, 044040 (2021).

[57] H. Sakhouf, M. Daoud, and R. A. Laamara, “Simple scheme for implementing the grover search algorithm with superconducting qubits,” *J. Phys. B* **54**, 175501 (2021).

[58] G. Anikeeva, O. Marković, V. Borish, J. A. Hines, S. V. Rajagopal, E. S. Cooper, A. Periwal, A. Safavi-Naeini, E. J. Davis, and M. Schleier-Smith, “Number partitioning with Grover’s algorithm in central spin systems,” *PRX Quantum* **2**, 020319 (2021).

[59] M. Lu *et al.*, “Multipartite entanglement in Rabi-driven superconducting qubits,” *PRX Quantum* **3**, 040322 (2022).

[60] Z. Wang, M. Pechal, E. A. Wollack, P. Arrangoiz-Arriola, M. Gao, N. R. Lee, and A. H. Safavi-Naeini, “Quantum dynamics of a few-photon parametric oscillator,” *Phys. Rev. X* **9**, 021049 (2019).

[61] D. F. James and J. Jerke, “Effective hamiltonian theory and its applications in quantum information,” *Can. J. Phys.* **85**, 625–632 (2007).

[62] A. Rauschenbeutel, G. Nogues, S. Osnaghi, P. Bertet, M. Brune, J. M. Raimond, and S. Haroche, “Coherent operation of a tunable quantum phase gate in cavity QED,” *Phys. Rev. Lett.* **83**, 5166–5169 (1999).